

The LiDAR-based topo-hydrological modelling of the Nigula mire, SW Estonia

Elve Lode^{a,b} and Meelis Leivits^c

^a Institute of Ecology, Tallinn University, Uus Sadama 5, 10120 Tallinn, Estonia

^b Department of Soil and Environment, Swedish University of Agricultural Sciences, P.O. Box 7014, Lennart Hjelms väg 9, SE-75007 Uppsala, Sweden; elve.lode@gmail.com

^c Environmental Board, Pärnu-Viljandi region, Vana-Järve, Tali 86107, Estonia; meelis.leivits@nigula.ee

Received 10 February 2011, accepted 22 June 2011

Abstract. There was no big influence of the used cell scales and algorithms on the mean topographical properties of the Nigula mire digital elevation models (DEMs). The DEMs, generated using the Triangulated Irregular Network and Inverse Distance Weighted algorithms, revealed the closest mire surface properties from all used generation algorithms. The subtracted MAX–MIN DEMs layer revealed a well visible net of ditches and possible plant cover pattern differentiated in vertical scale. In the Nigula mire 58% of the mire surface basins have S–SW orientation, followed by the levelled and less fractionated N–NE basin region (23% coverage), and the most fractionated but with steeper sloping W-orientated basin region (8% coverage).

Key words: mire landscape, LiDAR data, GIS, DEM analysis, basin modelling.

INTRODUCTION

Ground and surface water, in its specific dynamics, has a major role in the development of mire landscapes and their surface patterning. Already in the early 20th century it was reported that the vegetational patterning of raised bog was closely related to landform morphology and hydrology, advancing so the development of a three-dimensional and dynamic view of the raised bog development (Glaser 2002). Since then, the general term of *patterned peatland* or *patterned mire* has been used for sites with a specific type of pattern, formed by mire microforms for instance. They can be found on bogs, fens or a combination of the two (Rydin & Jeglum 2006).

Peatlands patterning is closely related to surface water discharge, not only across the mire boundary into the surrounding landscape, but also to the processes occurring within the mire which regulate the flow towards the boundary (Ingram 1983). In the case of elongated features of the mire surface pattern, usually stretched out perpendicular to the mire surface slopes, these processes can provide useful empirical information about the direction of the main flow paths in the mire area (e.g. Ivanov 1981; Rydin & Jeglum 2006). Price & Maloney (1994) concluded that the movement of water within, and out of, patterned peatlands is strongly controlled by the nature and position of pools and ridges

within the peatland water basin. In a patterned bog with relatively high ridges the ridges can act as local aquitards in the mire, hydrologically separating pools from each other and also causing the expansion of the depressions and storage of surface water retention in the area.

Changes in mire microtopography and in situ distribution of mire surface microforms or complexes of those (i.e. microtopes), together with the corresponding surface roughness properties, have been shown to be important hydro-topological factors in the formation of discharge components for the peatland catchments. The surface runoff or overland flow, seepage, groundwater and pipe flow, and open channel flow (i.e. rills, streams or even rivers), have been named as the key hydrological pathways of those catchments (e.g. Eggelsmann et al. 1993; Holden 2005).

However, because of patterned and at the same time comparably levelled surfaces the delineation of discharge-forming catchments on the peatlands is difficult (Ingram 1983; Eggelsmann et al. 1993). Adding for all, a *mire macro-landscape* (Galkina 1946, cited in Masing 1998) or a *system of mire massifs* (Ivanov 1981), or *mire complexes* (Moen 2002) surrounded by minerotrophic fens of variable extent, could consist of several *elementary mire massifs* (Galkina 1946, cited in Masing 1998), where the residual and secondary developed water bodies, lagg fen areas and mineral islands exist. Hydro-

logically these mire massifs in complexes are connected via different mire types and may contain *Carex* fens, wet forests, flat bogs and string mixed mires (Rydin & Jeglum 2006). Very often the general shape of a mire complex and its surface patterning also reflects interactions between the underlying mire terrain form (e.g. *paludified* mires), and the regional climate and hydrological environment of the peatland location (e.g. Ingram 1983).

About two thirds of Estonian mires have developed due to paludification of mineral land (incl. 30% of mire formation on sandy soils) (Allikvee & Ilomets 1995), and about one third have formed by ‘infilling’ of the surface water bodies, also called *terrestrialization* or *hydroseral succession* (e.g. Lode 1999). According to the general surface shape classification of elementary mire massifs, in Estonia there are mires with (1) flat or slightly convex sloping surfaces, sometimes located on the sites of spring upwellings, (2) flat or gently undulating surfaces of fens or transitional mires, i.e. poor fens, and (3) convex surfaces of bogs, which can be divided into (a) slightly convex surfaces with minimally segregated marginal slopes, (b) flat plateau surfaces with deep marginal slopes and (c) strongly convex surfaces with extensive and obvious marginal slopes (Masing 1988).

Currently, delineation of wetland basins and evaluation of water discharge dynamics are an important tool for integration of wetlands (incl. peatlands or mires) into the EU Water Framework Directive (EC 2003).

The LiDAR (short for Laser Imaging Detection And Ranging) data sets existing in Estonia provide high-quality three-dimensional surfaces of patterned peatlands and their delineated water basins. The availability of elevation data in digital format has favoured development of automated tools that can be used to delineate drainage basins and their associated stream network (Furnans & Olivera 2000). Accurate digital surface data, visualized via digital elevation models (DEMs), are the primary advance of LiDAR data, which are less subject to the horizontal error inherent in comparison of contour lines derived from ordinary contour maps (Haile 2005).

Krause & Bronstert (2005) expressed their doubts about the possibility of using algorithms of automatic digital terrain analysis for delineation of watersheds within lowland floodplains, because of a minimal extent of topographical heterogeneity required for the generation of DEMs. However, analysis of laser scanning of the fine-scale pattern along hydrological gradients in a peatland ecosystem has given promising results in a range of ecosystems where the vegetation pattern is linked to the ecological function (Anderson et al. 2010).

Many factors affect the accuracy of DEMs, i.e. the accuracy, density and distribution of the source data, the algorithms used for data interpolation and the DEM resolution (Liu et al. 2007; Liu 2008). Anderson et al. (2006) indicated that DEM horizontal resolution significantly influenced the level of reduction that LiDAR data sets could withstand, although for the satisfied soil-landscape models the DEM resolution could vary from 2 m resolution (Gessler et al. 2000) to 10 m and 30 m resolutions (Thompson et al. 2001). Results of the LiDAR DEM modelled flow network in Murphy et al. (2008) showed that the most accurate representation of the actual field-mapped network was even more accurate than the aerial photo-interpreted hydrographical data.

On the other hand, results of LiDAR-derived DEM modelling of the most important hydrological features, such as drainage network and boundaries of the sub-basin (also called basin or watershed), showed high sensitivity to both DEMs accuracy and the resolution used (Liu et al. 2005). However, it was demonstrated that the LiDAR-derived DEMs of high accuracy and high resolution offered the possibility of improving the quality of hydrological features derived from DEMs (*Ibid*).

The aims of this paper are (a) to compare the topographical properties of different LiDAR-derived DEMs (generated for different pixel sizes with different algorithms) for the Estonian Nigula mire complex, (b) to demonstrate the mire basin modelling results of different LiDAR-derived DEMs, (c) to compare the LiDAR-derived DEM modelling results with results derived from an empirical map at a scale of 1 : 10 000, constructed from results of earlier field measurement campaigns (presented in Raukas & Kink 1993/94) and (d) to define the most suitable topo-hydrological modelling approach for the Nigula mire landscape analysed.

MATERIAL AND METHODS

Study area

The Nigula mire is located on the Pärnu lowland, in the southwest of Estonia, 10 km to the east of the Gulf of Riga (Fig. 1). The peculiarity of the surface patterning of the contemporary Nigula mire is related to the origin of the mire formation. It began as an ‘infilling’ of Ancylus Lake during the Boreal period, first in the western part and thereafter in the eastern part of the lake (Pirrus 1963; Karmu 1966; Loopmann et al. 1988). About 8000–8500 years BP the western part of Ancylus Lake was ‘infilled’ by the mire. The terrestrialization of the eastern part of the lake started about 5000 years later,

i.e. 3000–3500 years BP (Raukas & Kink 1993/94). The NE–SW orientation of the current Nigula mire is defined by the orientation of the small-drumlin thresholds from the Ancylus Lake period, at present partly ‘buried’ under the mire, partly outcropping as small-drumlin residuals, forming mire mineral isles. Five outcropping mire isles occur in the current Nigula mire area, of which four, having the sequential NE–SW orientation, divide the mire into two parts – one third of the area is the western Urissaare bog and two thirds of the area make up the eastern Nigula bog (Kolla 1982) (Fig. 1).

A surface track depression of the previous Lemme River bed, beginning on the pool-ridge microtope in the middle of the Nigula bog, is located between the mineral island to the east and Lake Nigula to the west. The depression runs towards the SW corner of the Nigula mire. According to a field survey carried out in the middle of the 20th century, the Lemme River bed depression was hardly segregated on the bog surface (Karmu 1966), but in the undercut stream bed region the breadth of the stream bed was about 1.0 m and the depth about 0.5 m (Puura et al. 1990). The velocity of the open water river flow at its start was about 0.8 m/s, but increased towards the SW corner of the mire area up to 2.3–3.0 m/s (Karmu 1966).

The Nigula bog is a typical Estonian *southwestern large bog-type* bog with a flat plateau. The bog has a relatively steep 0.03–0.05‰ marginal slope in the east; the other marginal slopes vary slightly around 0.002‰ (Loopmann et al. 1988). The average slope of the southern oriented plateau is about 0.001–0.0015‰ (Karmu 1966). The western marginal slope of the Urissaare bog, contrary to that of the Nigula mire, is comparatively higher (2.3 m) and steeper (0.03–0.05‰), but both these values decrease towards the south. In the eastern part the bog is smoothly connected to the mineral island (Karmu 1966; Loopmann 1970) (Fig. 1).

The highest point of the Nigula mire is located in the northern part of the Urissaare bog (59.5 m a.s.l.) (Loopmann 1970). The average peat depth over the whole Nigula mire is about 3–5 m with a maximum of 6–7 m (Karmu 1966).

The prevailing *mire type* in the Nigula mire is the *bog*. Only mineral isles and narrow belts of the *transitional mire* skirt the dominating bog-type mire areas (Puura et al. 1990). However, two non-bog type parts exist in the Nigula bog area: (1) the NE ‘corner’ of the mire, called a *quaking* or *hag-type* mire (Loopmann 1970), and (2) the SE ‘corner’, where probably some hand peat-cutting took place at the beginning of the 20th century (Karmu 1966).

The main area of the present mire surface is fed by precipitation. The excess water from the overland flow

is collected in the belt areas between the mineral isles and the bog massifs, and upwelling of the *bog karstik springs* occurs not far to the east of the northern area of the mineral isles (Karmu 1966).

The Nigula mire is a water divide into four main surface water courses, called the Salatsi, Lemme, Häädemeeste and Rannametsa rivers. The Lemme and Häädemeeste rivers run out of the Nigula mire towards the SW, the Rannametsa River flows towards the NE and the Salatsi River in a SE direction (Karmu 1966). According to Loopmann (1970), the total length of the ditches surrounding the Nigula mire is about 17–25 km, the average breadth of which is 2 m and depth 1 m. The fluvial surface water runs into the ditches mainly during the spring and summer-autumn flooding periods.

The GIS-based study area, considered in this paper, forms 3845.10 ha (perimeter 26.08 km), covering the 2411.03 ha Nigula mire area (perimeter 35.34 km). The GIS study area is limited by roads to the north, east and south, whereas the eastern road follows the course of the Tuuliku drumlin ridge. In this study the Nigula mire itself, as a landscape, is defined by the ‘0’ contour line of the peat soils (Fig. 1).

The Nigula mire pools, with open water surfaces, have been classified as *hillside* and *water-divide* pools, *pool-lakes*, *depression* and *upwelling well pools*, and *river bed remnant* and *after-fire pools* (Karmu 1966). Currently the Nigula mire is covered with 1261 open water bodies of different sizes (i.e. Lake Nigula, pools and shallow inundated hollows) which were digitized manually from the orthophoto of the year 2005 at the beginning of the current study. The open water bodies cover a total of 71.78 ha (i.e. 3.0%) of the mire area, including the Lake Nigula area of 20.13 ha.

In the GIS-based study area the total length of fluvial water pathways, including ditches, is about 120 km, of which about 50 km (i.e. 41%) is located inside the mire border area, i.e. directly on the mire. The elevation difference between the highest Northwest section (60.83 m a.s.l.) and the lowest Southwest section (49.35 m a.s.l.) of the mire is 11.5 m. The longest longitudinal profile is about 9.5 km and the average breadth in the central part of the mire area is about 3.5 km (Fig. 1).

Creation of DEMs

The LiDAR data were used for different generated DEMs. The laser altimetry data used were gained from a Leica ALS50-II scanner device during a flight survey on 10 May 2008. The average flying height during the survey was 1 km and the resulting *First Echo point* density at nadir was expected to be 2.3 points/m². After

the data post-processing the vertical accuracy of the laser data points was determined to be 8 cm. The data point 'cloud' was then split into 500×500 m subsets and classified into *Overlap* and *Erratic High* and *Low* point classes with the *TerraScan* software. *LastEcho* points were used to generate the *Ground* point class, which was the basis for the generation of DEMs (Fig. 2). The ground point data density was determined to be 0.8 points/m². Using the Triangulated Irregular Network (TIN) and Inverse Distance Weighted (IDW) algorithm implementation in the *LP360* module (i.e. the LiDAR extension for *ArcGIS*, *RockWare Inc.*), several DEM surfaces with different pixel sizes (1×1 m, 2×2 m, 5×5 m, 10×10 m) were generated (later named as TIN or IDW DEMs).

The *Local Binning Algorithm* (Kim et al. 2006) with a standard *Search radius* (equals *cell resolution* $\times \sqrt{2}/2$ m, in our case the suggested cell resolution is 0.63 m), was used for the creation of MAX and MIN DEMs, whereby the maximum values track the highest elevation points, usually to the top of vegetation, and minimum values to the ground level surface (*Ibid*). Since all altimetry data were collected in the *GRS-80* height system, the surfaces were then normalized to a *Bk77* height reference system, using a geoid undulation of 19.75 m.

A total of ten LiDAR-based DEMs were generated for the following 3D surface analysis and *Hydrological Basin* modelling.

Empirical (EMP) DEMs were generated with the *ArcMap* software via the *TopoToRaster* module, whereas the elevation points for modelling were derived from a digitized empirical map layer at a scale of 1:10 000, constructed from results of earlier field campaigns and previously presented in Raukas & Kink (1993/94). In total four EMP DEMs of 5 m and 10 m cell resolution were created with differently defined *Ditch Feature Layers*, e.g. with and without SW ditches (Fig. 1). The used density of the *Contours* was 0.2 m in generation of EMP DEMs. The model network layers of *Streams* and *Roads* were extracted from the Estonian Base map and were elaborated with corresponding visualizations from the orthophoto of 2005 (Fig. 1). The *Lake* layer was obtained from manually digitized water bodies of the orthophoto 2005 layer (Lode et al. 2011).

All DEMs were created within the GIS-based *Study area* covering the whole Nigula mire landscape. A buffering belt was left between the net of the main road system and the mire '0' contour line (Fig. 1).

Topo-hydrological modelling

A *HillShade* module of the *ArcMap Version 9.3* software was used for visualization of all created DEMs

and the *ArcToolbox* package for modelling of the corresponding *Surface* and *Hydrology* layers. *Statsoft 2009* was used for presentation of comparative statistics of the generated DEM layers.

In *Basin* modelling the *ArcHydro Tools version 1.3 Final* as an extension for the *ArcGis 9.2/9.3* was used in *Depression Evaluation* of relevant DEMs. *Sink Depth* evaluation (i.e. maximum height differences of the cell 'gaps' inner surrounding cells) of DEM layers, used later for the *Basin* modelling, were performed via *Sink*, *Watershed*, *Zonal Statistics*, *Zonal Fill* and *Math Minus* modules of the *ArcMap* software (ESRI 2007). The *Default*, and 75%, 50%, 25% and 5% of maximum values of modelled sink depths were used for defining *Z limit* values for *pour point filling* in the relevant DEMs during the *Basin* modelling runs. *Basin* modelling with differentiated *Z limits*, together with the corresponding *Sink Depth* analysis, was applied to the two TIN DEMs with 5 m and 10 m cell resolutions.

MIN and MAX DEMs with 10 m cell resolution only were used both for the *Sink Depth* analyses and the *Basin* delineation runs.

RESULTS

Topographical characteristics of DEMs

All generated DEMs were visualized via the *HillShade* module. The *HillShade* layers of visualized 1 m, 2 m, 5 m and 10 m cell resolution DEMs revealed the cell size resolution-dependent mire surfaces, where the 1 m and 2 m cell resolution layers fitted well for visualization of mire micro-topography, and the 5 m and 10 m cell resolution layers for the whole mire landscape (Fig. 3), where manually digitized open water bodies from the orthophoto accord well to the micro-topographical structure of the visualized *HillShade* layers.

There was no noticeable cell scale dependence or generation algorithm impact on *General Statistics* of the modelled *Elevation* and *Aspect* layers for different DEMs over the whole mire landscape (Table 1); the *mean* aspect statistics of all model runs clearly depicted the southern orientation of the Nigula mire surface. *General Statistics* of the modelled *Slope* layers for the 1 m and 2 m cell resolution mire DEMs showed higher values, both for the *Slope max* and *Slope mean* values, in comparison with 5 m and 10 m cell resolution DEMs.

Similarly, no differences were observed in the visualized *Elevation* layers of the different DEMs, contrary to the modelled *Slope* layers. Almost none of the LiDAR-based *Aspect* layers had well-observed aspect orientations in the visualized layers. Only the

Table 1. *General Surface Statistics* of LiDAR-based TIN, IDW, MIN and MAX DEMs, and empirically derived EMP DEM of the Nigula mire. StD is standard deviation

DEMs, resolutions	Elevation, m (Bk77)					Slope, degrees			Aspect, degrees	
	Min	Max	Range	Mean	StD	Max	Mean	StD	Mean	StD
TIN										
1 m	49.47	61.26	11.79	56.37	2.08	32.2	2.2	1.58	180.2	102.5
2 m	49.47	61.24	11.77	56.37	2.08	25.6	1.3	0.98	180.5	101.6
5 m	49.48	61.26	11.78	56.37	2.08	15.1	0.63	0.55	180.3	99.5
10 m	49.92	60.82	10.90	56.37	2.08	6.36	0.42	0.40	180.2	96.7
IDW										
2 m	49.42	61.29	11.87	56.37	2.08	36.1	1.3	1.01	179.8	101.7
5 m	49.48	61.24	11.76	56.37	2.08	16.5	0.58	0.54	180.1	98.9
10 m	49.78	60.87	11.09	56.37	2.08	6.33	0.38	0.40	180.3	95.5
MIN										
10 m	49.66	60.48	10.82	56.20	2.09	8.70	0.34	0.47	181.2	92.9
MAX										
10 m	50.37	61.33	10.96	56.57	2.07	5.18	0.37	0.37	181.3	95.2
EMP*										
5 m	49.14	60.33	11.19	56.15	2.09	13.2	0.31	0.55	177.6	89.3
EMP*										
10 m	49.60	60.84	11.24	56.11	2.17	15.9	0.41	0.95	175.7	88.2

* All main SW-oriented ditches were included into the *TopoToRaster* module run.

Reclassified Aspect layer to the five classes of 10 m cell resolution DEMs resulted in a visibly meaningful mire surface orientation pattern.

On average, the EMP DEM *Elevation* and *Slope* layers showed the lowest surface property values in comparison with LiDAR-derived DEMs (Tables 1 and 2). The surface *mean Aspect* of the EMP DEM was the most eastern oriented and the visualized *Aspect* layer

had the coarsest, but most easily observed surface cell-aspect orientations of all the modelled DEMs (Fig. 4).

Although there was no clear differentiation in general statistics of the EMP DEM from altimetry-generated DEMs of 10 m cell resolution (Fig. 5), differences were observed in the tree cluster results (Fig. 6), where the *Linkage Distance d* was shortest between the TIN and IDW DEM data sets ($d = 19$), and the longest between data sets of LiDAR-derived MAX DEM and the EMP DEM ($d = 209$ in Table 3).

Table 2. Differences in *General Statistics* between empirical (EMP) and altimetry-derived TIN, IDW, MIN and MAX DEMs at 10 m cell resolution. The number of cells was $N = 241\ 092$ for each DEM layer, and *Subtr. DEMs are subtracted layers of the corresponding DEMs

*Subtr. DEMs	Elevation, m (Bk77)			
	Mean	StD	Min	Max
EMP-TIN	-0.16	0.27	-1.86	1.71
EMP-IDW	-0.14	0.26	-1.87	1.90
EMP-MIN	-0.04	0.26	-1.50	2.11
EMP-MAX	-0.34	0.26	-2.29	1.16

Table 3. Matrix of Euclidean distance results of empirical (EMP) and altimetry-derived TIN, IDW, MIN and MAX DEMs at 10 m cell resolution, where the number of cells was $N = 241\ 092$ for each DEM layer

DEMs	EMP	TIN	IDW	MAX	MIN
EMP	0	151	142	209	127
TIN	151	0	19	102	122
IDW	142	19	0	115	107
MAX	209	102	115	0	197
MIN	127	122	107	197	0

Results of agglomeration of DEMs into the tree diagram clearly depict the high similarity of LiDAR-derived IDW and TIN DEMs. According to the Euclidean distance matrix, the EMP DEM model had the shortest distance with the MIN DEM model ($d = 127$).

Basins of delineated DEMs

Results of the *Basin* delineation of Nigula mire EMP DEMs showed a significant dependence on the ditch features used in modelling runs (Fig. 7). Due to different inputs used for the *Ditch Feature Layer* in two basin modelling runs, the areal difference for the southern Nigula mire basins constitutes 5.6%, 44.5% and 62.8% (Table 4 and Fig. 7). At the same time, the sum of areal coverage of those basins had differed only by 3.5%, i.e. 62.08 ha.

Study of *Sink depths* of TIN DEMs at cell resolutions of 5 m and 10 m showed that the main areas with high values (e.g. *Sink Depths* equals 2.04 m for the TIN DEMs at cell resolution of 5 m, and equals 1.38 m at 10 m cell resolution) were concentrated on the main ditch locations. The mean values were found at the sites with tree or shrub coverage and the lowest values were found in the open mire areas (Fig. 8).

Basin model runs of LiDAR-derived 10 m cell resolution TIN DEMs revealed increment of the delineated basin count from 34 to 95 by the change

of $Z(\text{limit})$ from $Z(\text{limit}) \text{ equals } \text{max}$ to $Z(\text{limit}) \text{ equals } 25\% \text{ of the } \text{max value}$, and for the 5 m cell resolution from 31 to 55 by the same $Z(\text{limit})$ value changes (Fig. 9).

On the other hand, the counts of the modelled basins were rather similar for the TIN DEMs at cell resolutions of 5 m and 10 m (31 and 34 respectively) by the used $Z(\text{limit}) \text{ equals the } \text{max value}$. In the case where the $Z(\text{limit}) \text{ equals } 25\% \text{ of the } \text{max value}$ the differences between modelled basin counts at cell resolutions of 5 m and 10 m reached 42% (i.e. 40 basins). Although differently modelled basin layers had different basin counts and basin shapes, there was one main (the largest) basin, delineated from the 10 m cell resolution TIN DEM *Basin* run, which could be easy to aggregate to almost the same shape and extension, similarly to the EMP DEM *Basin* run results (Fig. 7), by summarizing the catchments from the other *Basin* runs (Fig. 9).

The delineated basins for the MIN DEM 10 m cell resolution *Basin* run were visually similar to the basin delineation at a 5 m cell resolution TIN DEM, and for the MAX DEM 10 m cell resolution *Basin* run, to the 10 m cell resolution TIN DEM *Basin* run (Figs 8 and 10). This indicates the better ‘reflection’ of the finer-scale surface patterning in the MIN DEM layer (although with a lower 10 m cell resolution) in comparison with the MAX DEM layer. All these described *Basin* runs were performed with *max* or *Default Z(limit)* in the *Surface Filling* procedure before the *Basin* runs.

It could be stated that there were four main basin regions which could be defined from all *Basin* runs by the $Z(\text{limit}) \text{ equals } \text{Default}$ values for all used DEMs: (1) basin region with a north to northeastern orientation, with a total drainage area of about 560 ha (the minimum number of modelled sub-catchments is 3); (2) basin region with a south to southwestern orientation, with a total drainage area of about 1400 ha (the minimum number of modelled sub-catchments is 11); (3) basin region with an east to southeastern orientation, with a total drainage area of about 270 ha (minimum number of modelled sub-catchments is 4); and (4) basin region with a western orientation, with a total drainage area about 180 ha (minimum number of modelled sub-catchments is 17) (Fig. 11). From all the main basin regions the basins with S–SW orientation cover about 58% of the total mire surface area, followed by the N–NE region basins with 23% coverage, E–SE region basins with 11% coverage and W-orientated basins with 8% coverage. The most fractionated basin region is the W region and the least fractionated is the N–NE region.

Table 4. Results of two EMP DEM *Basin* modelling runs for the southern part of the Nigula mire. Depending on *Ditch Feature Layer* inputs used, in the *Basin 1* layer SW ditches were included and in the *Basin 2* layer not included in the model run (see also Fig. 7). The cell resolution of input EMP DEMs was 5 m, and 10 m cell resolution was used in the output of delineated *Basin* layers

Basin modelling runs				Difference, %
With SW ditches (<i>Basin 1</i> layer)		Without SW ditches (<i>Basin 2</i> layer)		
Modelled basins, No.	Area, ha	Modelled basins, No.	Area, ha	
1	1261.69	1	1191.06	5.6
2	417.67	4	231.92	44.5
5	115.20	3	309.50	62.8
Total	1794.56	Total	1732.48	3.5

CONCLUSIONS

The LiDAR data application to the patterned mire landscape in Estonia demonstrated both advantages and challenges of the study of different DEMs, generated directly from the LiDAR raw data material. Not all modelling output results, concerning the influence of different DEMs that used cell sizes and algorithms on different mire topographical and hydrological properties, were presented in the current study, and no ground-level validation was carried out. However, there is a possibility of outlining some general trends covering the research objectives formulated at the beginning of the study.

It has been shown that there were no significant differences in mean values calculated for *Elevation* and *Aspect* layers of different LiDAR-derived DEMs for the whole Nigula mire landscape. Thus, in the landscape scale, any of the DEMs could be used for general topographical characterization of the mire surface. However, from a practical point of view (e.g. time and costs), the lower 5 m or 10 m resolution DEMs would be preferred in the case of the Nigula mire.

The *HillShade* layers, used for *hypothetical illumination* (ESRI 2007) of generated DEMs, demonstrated clearly the cell resolution-dependent mire surface results, where the DEMs of 1 m and 2 m cell resolution have a great perspective for fulfilling the traditional microstructural study demands on the mire area (Lode et al. 2011). Afterwards it could be concluded that the generated *HillShade* layers could also be taken as an indicator of the possible cell size scale limits in water basin delineation for the entire mire landscape.

Cell-based evaluation of all generated DEMs depicted higher similarities for the LiDAR-based TIN and IDW DEMs, whereas the generated EMP DEM had the smallest Euclidean distance with MIN DEM. This indicates that MIN DEM can be considered the most suitable DEM generation from LiDAR data sets for substitution of ‘ground level’ EMP DEM. At the same time the largest Euclidean distance of EMP DEMs from all LiDAR-based DEMs indicates that the empirical elevation map of the Nigula mire reflected less the mire micro-topographical pattern, since the *zero level* of

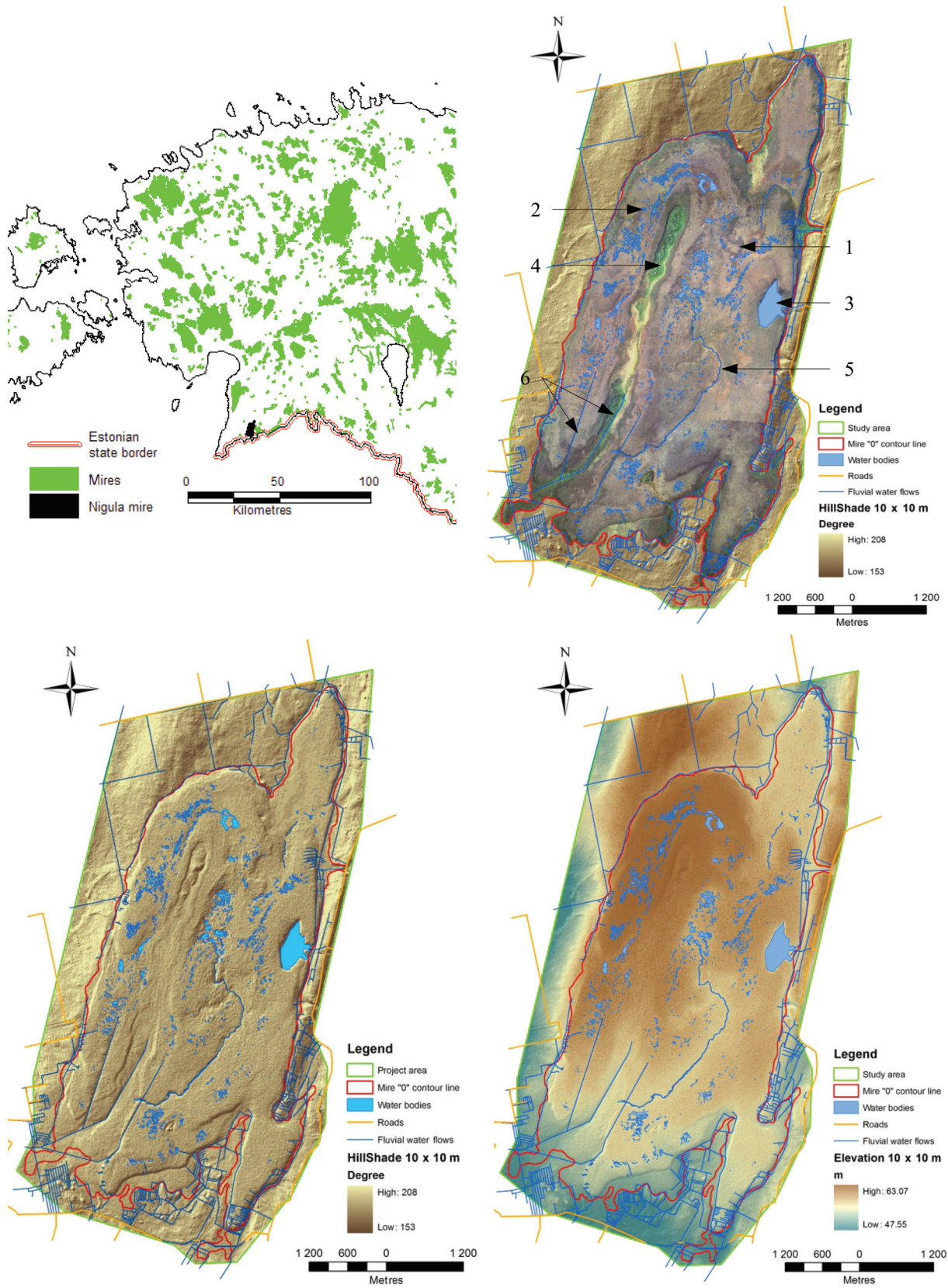
the mire surface was equalled to the heights of the hummock microform foots (Nastavlenie... 1972) during the field levelling campaign (Raukas & Kink 1993/94).

On the basis of all TIN DEM *Basin* runs it could be concluded that, at the landscape-scale level, the delineation and count of the modelled mire surface basins are cell resolution and *pour point* filling property (i.e. *Z(limit)*) sensitive. Although the *Filling of Sinks* for the *Basin* runs is used for removing a ‘...small imperfection...’ in the surface raster data (in the *Help* section of *ArcMap*), in the LiDAR data case used, the differentiated *Sink Depths*, i.e. *Z(limit)* equals 25%, 50% or 75% of *Sink Depth (max)*, could be regarded instead as modelling options for exercise scenarios of different mire hydrological conditions. In this case, for example, the *Basin* layers generated by the *Z(limit) equals Default* (i.e. equals the maximum value of the *Sink Depths* of the DEM), can be seen as a basin delineation scenario at the highest groundwater level conditions on the mire landscape. But such an approach relies on the assumption of correct raster DEMs generated from LiDAR data.

Subtracted MAX and MIN DEMs of 10 m cell resolution resulted in a well distinguished net of ditches and areal scattered patterning with a height amplitude between 0.00 and 3.54 m, indicating a possible relationship to tree and other higher plant cover distribution in the area with high values and to open areas with the plant cover from the field layer with low values. These results seem to be promising for GIS-based identification of plant cover distribution over the mire landscape in the vertical scale.

Two *Basin* modelling scenario runs display delineated mire basins with water divide location on the western border line of the Nigula bog and between the Lemme River bed depression and the same mire western border line. The basins were revealed from the *Basin* run of 10 m cell resolution MIN DEM (Fig. 10) and 5 m cell resolution TIN DEM by the used *Sink Depth equals Sink Depth (max)* values (Fig. 9). This could be taken as an indication of correct basin delineation results revealed by the natural mire surface pattern.

Fig. 1. Basic images of the Nigula mire GIS study area. The first image (top left) shows the location of the Nigula mire on the mire distribution map of Estonia (extracted from the electronic Base map of 1:50 000), the second image (top right) is the orthophoto of the Nigula mire (extracted from the standard orthophoto of the Estonian Land Board 2005), where roads, streams and ditches were identified after the Estonian Base map and the mire ‘0’ contour line was taken from the Estonian Soil map. The orthophoto with the 0.5 m cell resolution is overlain by the 10 m cell resolution TIN DEM *HillShade* layer (lower left image). The fourth image (lower right) is the 10 m cell resolution TIN DEM *Elevation* layer of the GIS-based study area. Both *HillShade* and *Elevation* layers were generated from LiDAR-based TIN DEM with a 10 m cell resolution. In the orthophoto image: 1, Nigula bog; 2, Urissaare bog; 3, Lake Nigula; 4, Salupeaksi small-drumlin threshold; 5, Lemme River bed track depression; 6, main ditches in the SW part of the Nigula mire.



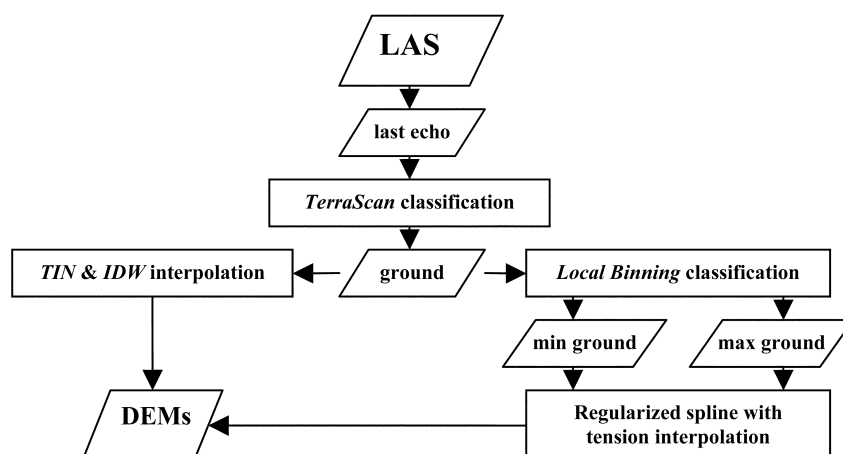


Fig. 2. Block scheme for generation of digital elevation models (DEMs) from laser altimetry data (LAS). Rectangles and rhombi represent procedures and datasets, respectively.

From all *Basin* runs it could be concluded that, in spite of considerable variation between the basin delineation, and counts from different modelling runs, there were some general, prevailing delineation, which could be easily aggregated from *Basin* runs with higher basin count results. Therefore, the selection of one or other *Basin* run result, as the final decision option, depends on the set up of the scale of the study area extension, e.g. the whole mire landscape or specific ecotopes or microtopes.

In summary, we can draw the following conclusions:

1. On the landscape scale the surface properties of the Nigula mire are well presented on LiDAR-based TIN and IDW DEM analysis results with cell resolutions of 5 m or 10 m.
2. It is not yet clear which of the used algorithms reveals the most reliable results for the ecotope surface studies by the 1 m or 2 m cell resolution DEMs.
3. The layer of subtracted MAX and MIN DEMs is a promising tool for the GIS-based visualization of the net of the linear objects (e.g. ditches) together with plant cover distribution on vertical scale.
4. The *Basin* run results of *ArcMap9.3* with *Default Sink Depths* can be taken as a basis for the ground-level study related to the delineation of the prevailing sub-basins on the Nigula mire landscape.
5. Analysis of four altimetry-derived DEMs and one ground-level-derived topological EMP DEM demonstrated that TIN and IDW DEMs provide with each

other the closest results in comparison with MIN, MAX and EMP DEMs, whereas the MIN DEM is the best among all generated DEMs for substitution of EMP DEM.

6. However, in suitable conditions the EMP DEM can be used for preliminary mire surface study before ordering the LiDAR scanning for a non-studied mire landscape.
7. Scale-based accuracy and resolution of DEMs are a crucial issue in relation to simulation and visualization of the morphological and hydrological properties of the mire surface.
8. Since the detailed man-made topological and eco-hydrological measurements of different mire complexes are usually labour-consuming, expensive and limited by the man-capability and skills, the results of remote sensing products must be used in mire landscape research.
9. The laser altimetry can be considered as the most accurate technology for the generation of detailed 3D DEMs for relatively flat but patterned mire surfaces.

Acknowledgements. This work was prepared in the framework of the Estonian research foundation project of SF0280009s07 ‘Impact of disturbances on wetland ecosystems in Estonia’ in collaboration with the Environmental Board and the Swedish University of Agricultural Sciences (Department of Soil and Environment). The authors would like to express their gratitude to the Estonian Land Board for making available electronical data sets and LLC ALPHAGIS for the helpful *ArcMap* related consultations.

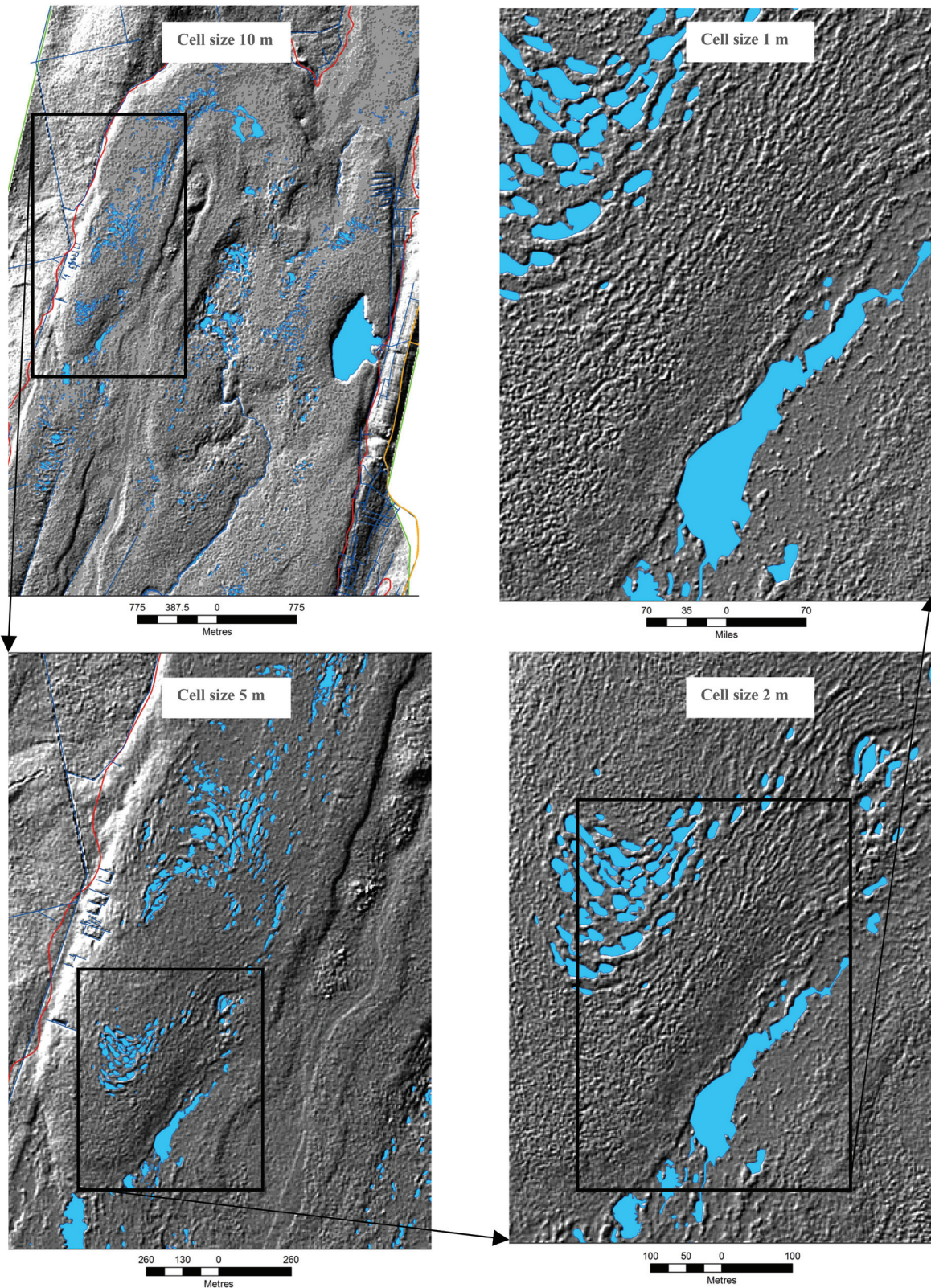


Fig. 3. Extractions of *HillShade* layers of the Nigula mire TIN DEMs with 10 m, 5 m, 2 m and 1 m cell resolutions. Black squares with arrows show the extensions to the next extraction with a smaller cell resolution. DEMs for all resolutions were generated from LiDAR data sets by using the TIN algorithm. Visualized water bodies (blue polygons on images) were digitized manually from the orthophoto of 2005.

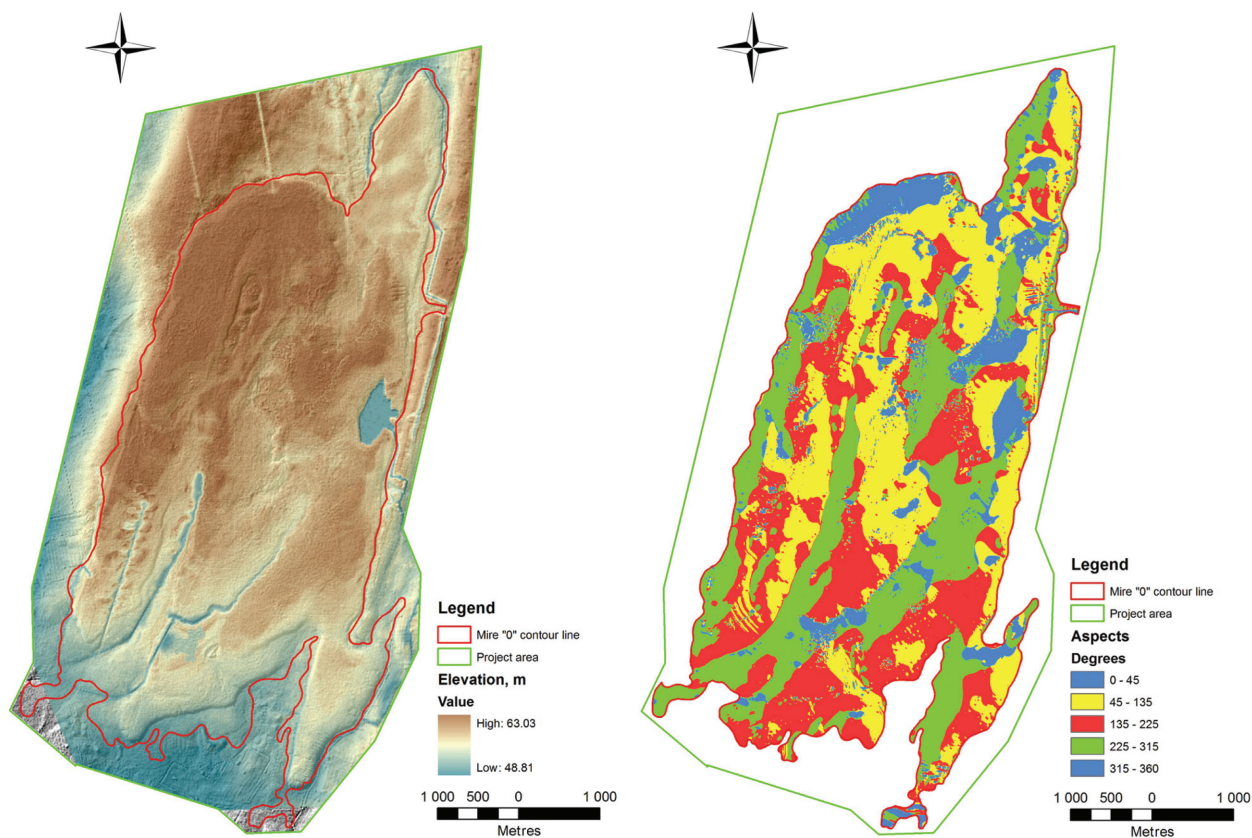


Fig. 4. Elevation and Aspect layers with the cell resolution of 5 m of the Nigula mire EMP DEM, generated from field surface levelling data (digitized from Raukas & Kink 1993/94). The density of mire surface contour lines before GIS modelling was 0.2 m and EMP DEM cell resolution was 5 m.

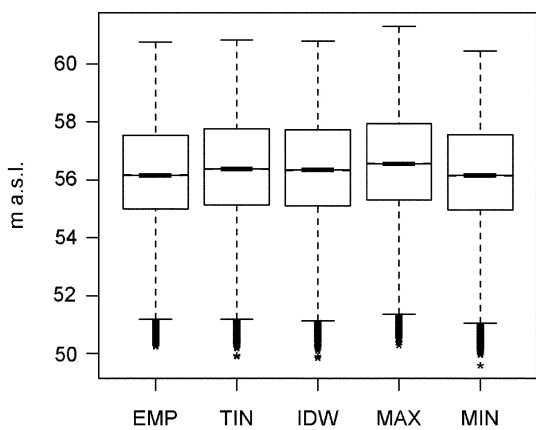


Fig. 5. Box plots of generated 10 m cell resolution EMP, TIN, IDW, MAX and MIN DEM Elevation layers with the total cell number of $N = 241\,092$ for each layer. The box represents the inter-quartile data range of 25–75%, the line in the box shows medians, whiskers denote min–max of the data range and stars outside the ends mark outliers.

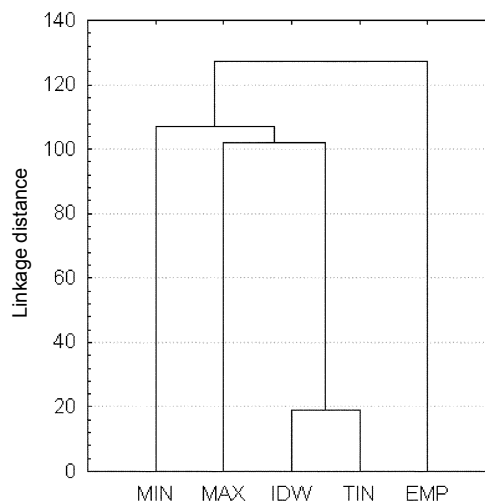


Fig. 6. Tree diagram of cluster analysis depicting the linkage distances between five DEMs of 10 m cell resolution with the cell number of $N = 241\,092$ for each DEM used in the analysis.

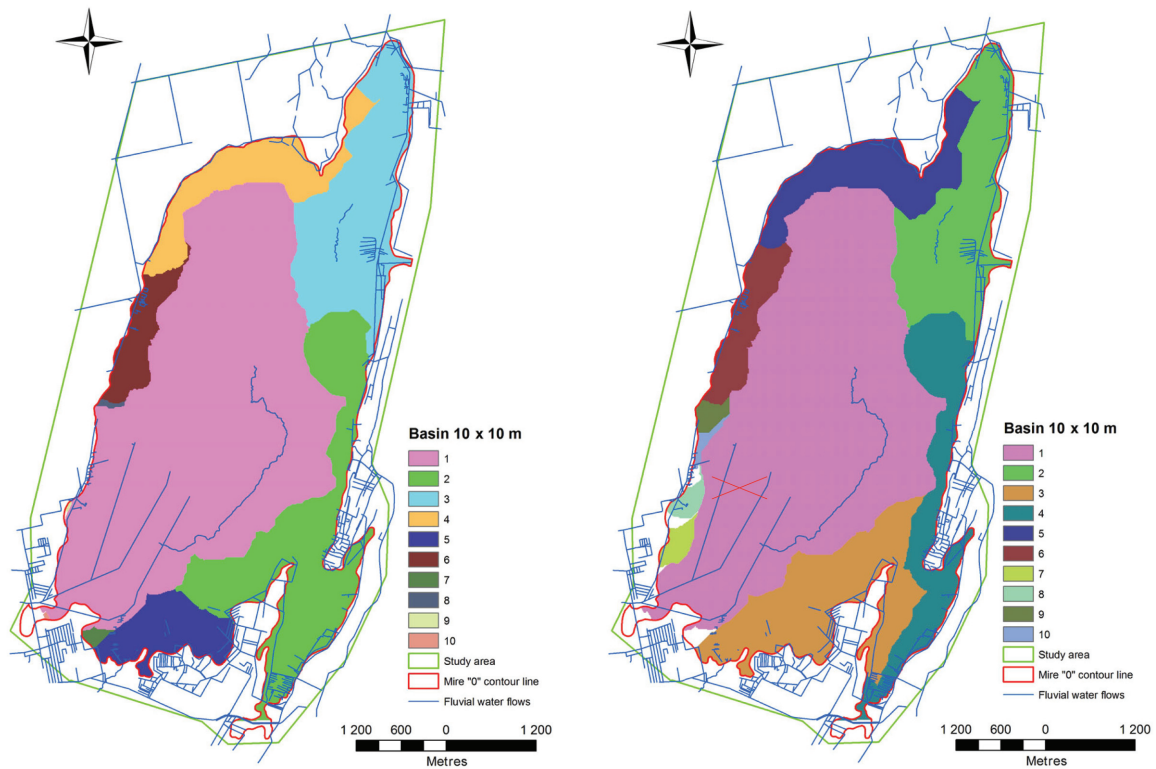


Fig. 7. Results of reclassified to ten basins of two *Basin* runs for the Nigula mire EMP DEM layer (used $Z(\text{limit}) = \text{Default}$). Depending on *Ditch Feature Layer* inputs used, in the *Basin 1* layer (left image) SW ditches were included and in the *Basin 2* layer (right image) ditches were not included in the model run. The cell resolution was 5 m for both EMP DEM inputs and 10 m in the output of delineated *Basin* layers.

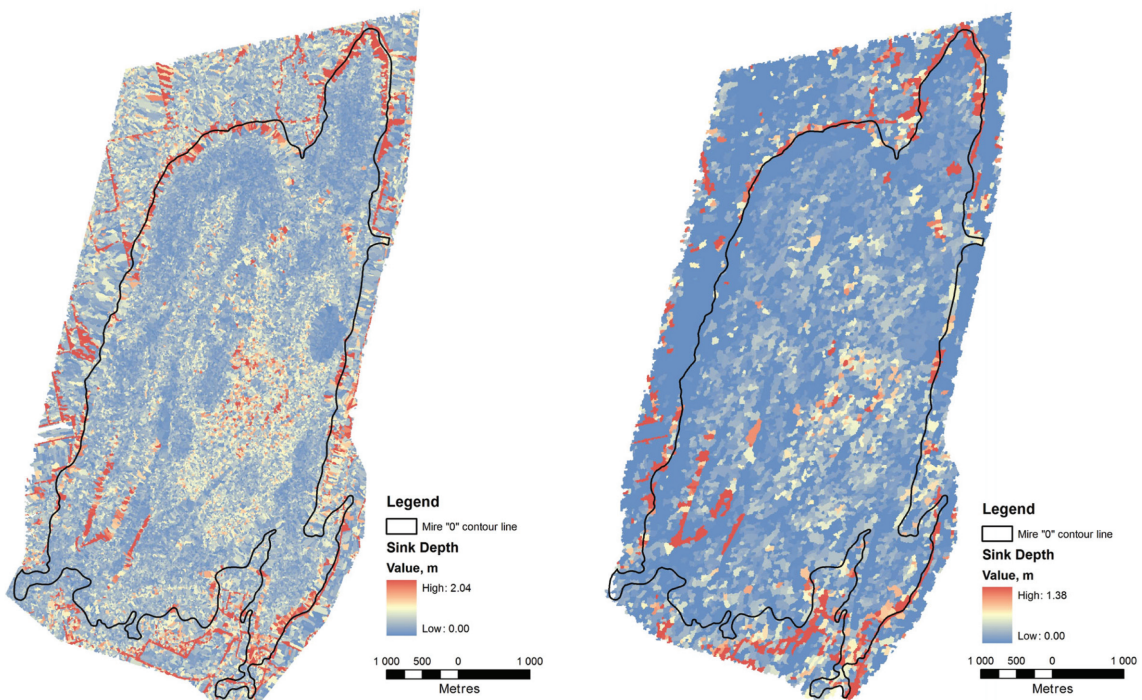


Fig. 8. Results of the *Sink Depth* study of 5 m (left image) and 10 m (right image) cell resolution TIN DEMs. The high values of the sink depths (pink pixels on images) concentrated on locations of the most ‘segregated’ parts of the ditches. The number of the sink cells $N = 55\,231$ for the 5 m cell resolution layer and $N = 8520$ for the 10 m cell resolution layer.

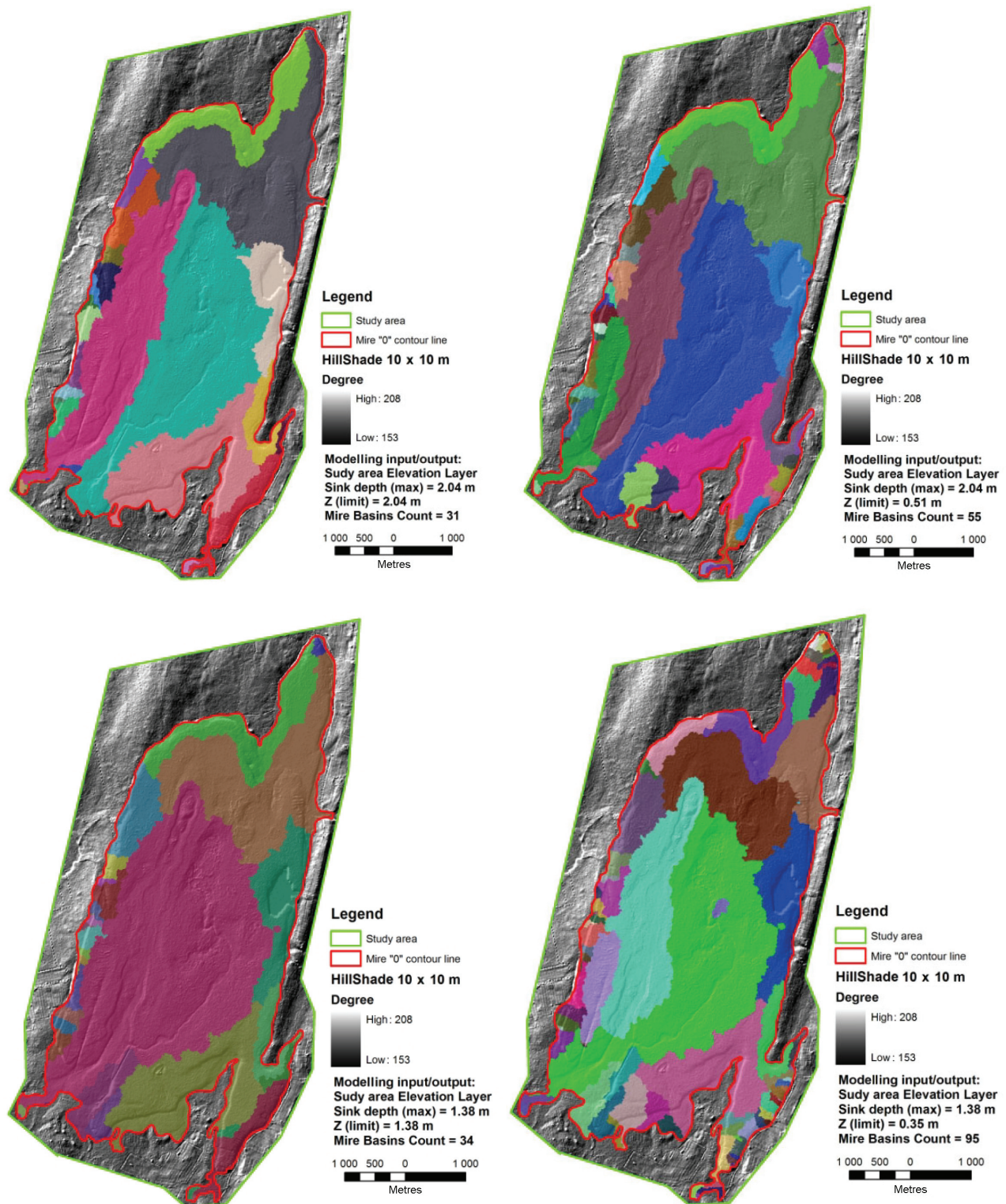


Fig. 9. Examples of delineated mire basins for the LiDAR-based TIN DEMs of 5 m (upper images) and 10 m (lower images) cell resolution, obtained by using $Z(\text{limit})$ values equalling the layer $\text{Sink Depth}(\text{max})$ (upper and lower left images) and Sink Depth 25% from the $\text{Sink Depth}(\text{max})$ values (upper and lower right images).

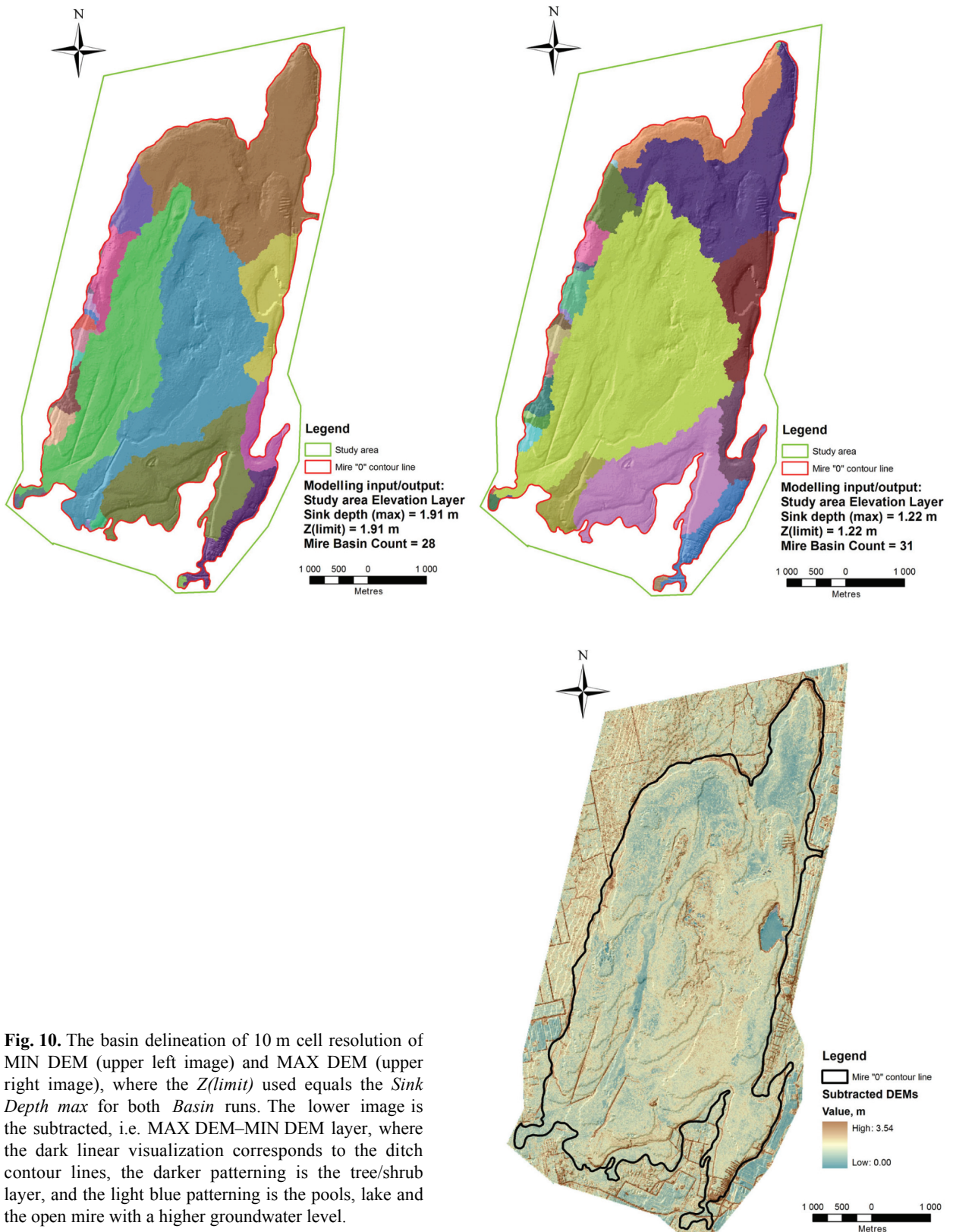


Fig. 10. The basin delineation of 10 m cell resolution of MIN DEM (upper left image) and MAX DEM (upper right image), where the $Z(\text{limit})$ used equals the Sink Depth max for both *Basin* runs. The lower image is the subtracted, i.e. MAX DEM–MIN DEM layer, where the dark linear visualization corresponds to the ditch contour lines, the darker patterning is the tree/shrub layer, and the light blue patterning is the pools, lake and the open mire with a higher groundwater level.

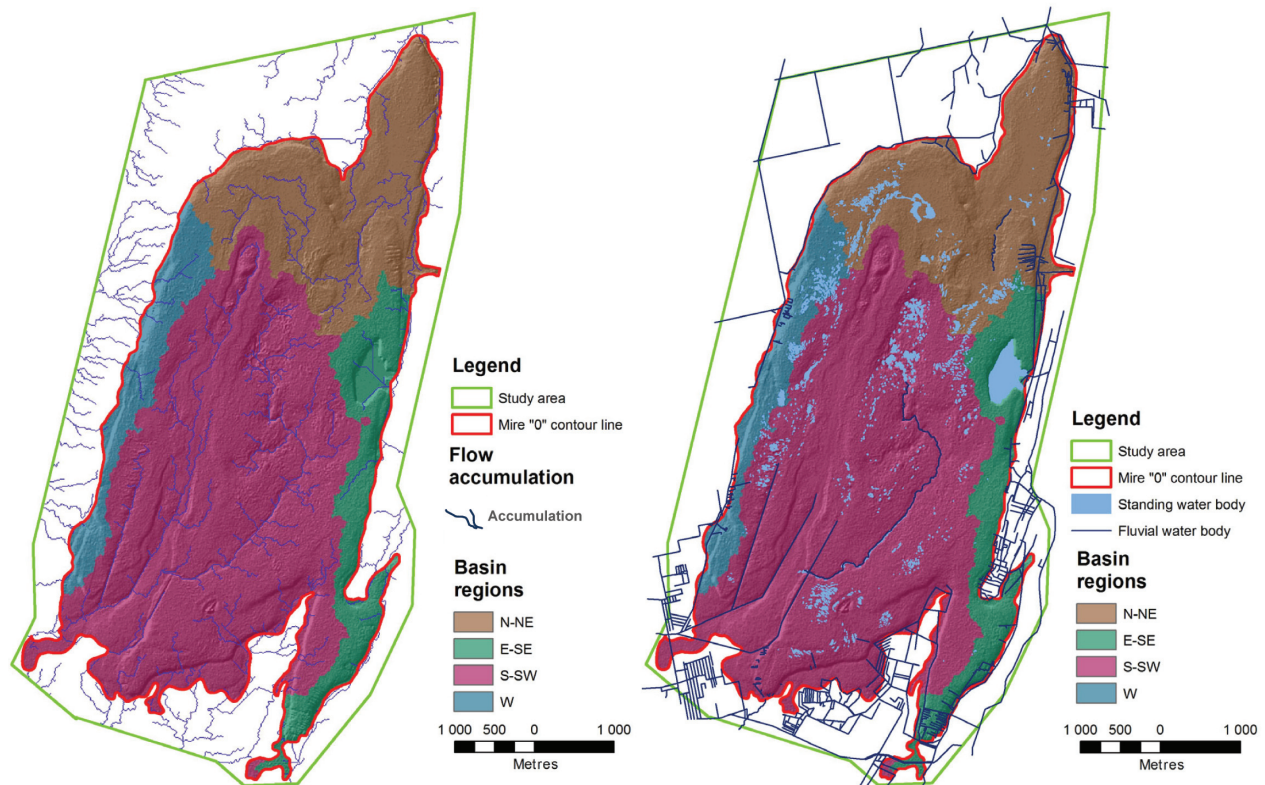


Fig. 11. Main basin regions of the Nigula mire landscape together with modelled flow accumulation (image on the left) and manually identified net of fluvial and standing water bodies from the orthophoto of 2005 (image on the right). The *Basin* layer with a 10 m cell resolution was generated from LiDAR-based TIN DEM with a 10 m cell resolution.

REFERENCES

- Allikvee, H. & Ilomets, M. 1995. Sood ja nende areng [Mires and their development]. In *Eesti Loodus [Estonian Nature]* (Raukas, A., ed.), pp. 327–346. Valgus, Eesti Entsüklopeediakirjastus, Tallinn [in Estonian].
- Anderson, E. S., Thompson, J. A., Crouse, D. A. & Austin, R. E. 2006. Horizon resolution and data density effects on remotely sensed LIDAR-Based DEM. *Geoderma*, **132**, 406–415.
- Anderson, K., Bennie, J. & Wetherelt, A. 2010. Laser scanning of fine scale pattern along a hydrological gradient in a peatland ecosystem. *Landscape Ecology*, **25**, 477–492.
- [EC] European Communities. 2003. Guidance Document No. 12 2003. *Horizontal Guidance on the Role of Wetlands in the Water Framework Directive*. Office for Official Publications of the European Communities.
- Eggelsmann, R., Heathwaite, A. L., Grosse-Braukmann, G., Küster, E., Naucke, W., Schuch, M. & Schweickle, V. 1993. 4. Physical processes and properties of mires. In *Mires. Process, Exploitation and Conservation* (Heathwaite, A. L. & Göttlich, Kh., eds), pp. 171–262. Wiley, New York.
- ESRI 2007. *Working with ArcGIS Spatial Analyst*. United States of America.
- Furnans, J. & Olivera, F. 2000. Chapter 4. Catchments and Watersheds. In *ArcGIS Hydro Data Model. Draft Data Model and Manuscript* (Maidment, D. R., ed.). GIS in Water Resources Consortium. ESRI & CRWR <http://www.crwr.utexas.edu/gis/gishydro00/ArcGIS/Chapter4/chapter4.pdf> [accessed 4 May 2011].
- Galkina, E. A. 1946. Bolotnye landschafty i printsipy ikh klassifikatsii [Mire landscapes and principles of their classification]. *Sbornik Nauchnykh Rabot Botanicheskogo Instituta Imeni V. L. Komarova, AN SSSR*, 139–156 [in Russian].
- Gessler, P. E., Chadwick, O. A., Chamran, F., Althouse, L. D. & Holmes, K. W. 2000. Modeling soil-landscape and ecosystem properties using terrain attributes. *Soil Science Society America Journal*, **64**, 2046–2056.
- Glaser, P. H. 2002. C. A. Weber’s benchmark treatise on the Augstumal Raised Bog: reflections on its significance and impact on peatland ecology. In *C. A. Weber and the Raised Bog of Augstumal* (Couwenberg, J. & Joosten, H., eds), Grif & K, 278 pp.
- Haile, A. T. 2005. *Integrating Hydrodynamic Models and High Resolution DEM (LIDAR) for Flood Modelling*. Thesis of International Institute For Geo-Information Science and Earth Observation Enschede, The Netherlands, 75 pp.

- Holden, J. 2005. Peatland hydrology and carbon release: why small-scale process matters. *Philosophical Transactions of the Royal Society A*, **363**, 2891–2913.
- Ingram, H. A. P. 1983. Hydrology. In *Mires: Swamp, Bog, Fen, and Moor: General Studies* (Gore, A. J. P., ed.), *Ecosystems of the World*, **4A**, 67–158. Elsevier, Amsterdam.
- Ivanov, K. E. 1981. *Water Movement in Mirelands*. Academic Press, London, 276 pp.
- Karmu, L. 1966. *Nigula Riikliku Looduskaitseala füüsilis-geograafiline ülevaade [Physico-geographical Overview of the Nigula State Nature Reserve]*. Unpublished graduation thesis, University of Tartu, Tartu, 110 pp [in Estonian].
- Kim, H. S., Arrowsmith, J. R., Crosby, C. J., Jaeger-Frank, E., Nandigam, V., Memon, A., Conner, J., Baden, S. B. & Baru, C. 2006. An efficient implementation of a local binning algorithm for digital elevation model generation of LiDAR/ALSM Datasets. *EOS: Transactions of the American Geophysical Union*, *87*, **52**, Fall Meet. Suppl., Abstract G53C-0921.
- Kolla, E. 1982. Peaksid piiramisrõngas [Besieged mire areas]. *Eesti Loodus*, **11**, 712–719 [in Estonian].
- Krause, S. & Bronstert, A. 2005. An advanced approach for catchment delineation and water balance modelling within wetlands and floodplains. *Advances in Geosciences*, **5**, 1–5.
- Liu, X. 2008. Airborne LiDAR for DEM generation: some critical issues. *Progress in Physical Geography*, **32**, 31–49.
- Liu, X., Peterson, J. & Zhang, Z. 2005. High-resolution DEM generated from LiDAR data for water resource management. In *Proceedings of International Congress on Modelling and Simulation 'MODSIM05', 12–15 December 2005, Melbourne, Australia*, pp. 1402–1408.
- Liu, X., Zhang, Z., Peterson, J. & Chandra, S. 2007. The effect of LiDAR data density on DEM accuracy. In *Proceedings of International Congress on Modelling and Simulation (MODSIM07), Christchurch, New Zealand*, pp. 1363–1369.
- Lode, E. 1999. Wetland restoration: a survey of options for restoring peatlands. *Studia Forestalia Suecica*, Swedish University of Agricultural Sciences, Faculty of Forestry, Uppsala, Sweden, 30 pp.
- Lode, E., Roosaare, J. & Pensa, M. 2011. Chapter 26: Typological up-scaling of wooded peatlands. In *Forest Management and the Water Cycle. An Ecosystem-Based Approach. (26)* (Bredemeier, M., Cohen, S., Godbold, D. L., Lode, E., Pichler, V. & Schleppei, P., eds), *Ecological Studies*, **212**, 471–496. Springer.
- Loopmann, A. 1970. *Nigula raba. Nigula Riiklik Looduskaitseala [Nigula Mire. Nigula State Nature Reserve]*. Tallinn, 36 pp. [in Estonian].
- Loopmann, A., Pirrus, R. & Ilomets, M. 1988. Nigula Riiklik Looduskaitseala. In *Eesti Sood [Estonian Mires]*. (Valk, U., ed.), pp. 227–233. Valgus, Tallinn [in Estonian].
- Masing, V. 1988. 2.4.3. Eesti soode liigitus [Classification of Estonian Mires]. In *Eesti Sood [Estonian Mires]*. (Valk, U., ed.), pp. 69–76. Valgus, Tallinn [in Estonian].
- Masing, V. 1998. *Multilevel Approach in Mire Mapping, Research, and Classification*. Contribution to the IMCG Classification Workshop, March 25–29, 1998, Greifswald, 6 pp.
- Moen, A. 2002. Mires and peatlands in Norway: status, distribution, and nature conservation. In *Third International Symposium on the Biology of Sphagnum. Uppsala–Trondheim, August 2002: Excursion Guide* (Thinggaard, K. & Flatberg, K. I., eds), pp. 41–60. Norges teknisk-naturvitenskaplige universitet, Vitenskapsmuseet, Trondheim.
- Murphy, P. N. C., Ogilvie, J., Meng, F.-R. & Arp, P. 2008. Stream network modeling using lidar and photogrammetric digital elevation models: a comparison and filed verification. *Hydrological Processes*, **22**, 1747–1754.
- Nastavlenie... 1972. *Nastavlenie gidrometeorologicheskimi stantsiyami i postami [Directions for Hydrometeorological Stations and Posts]*. Vypusk 8. Glavnoe Upravlenie Gidrometeorologicheskoy Sluzhby pri Sovete Ministrov SSSR. Gidrometeoizdat, 296 pp. [in Russian].
- Pirrus, R. 1963. History of the development of the Nigula raised bog. *ENSV TA Geoloogia Instituudi Uurimused*, **XII**, 163–173 [in Russian].
- Price, J. S. & Maloney, D. A. 1994. Hydrology of a patterned Bo-Fen complex in Southeastern Labrador, Canada. *Nordic Hydrology*, **25**, 313–330.
- Puura, V., Raukas, A. & Kink, H. 1990. *Vee Seisundi Kompleksne Ökoloogiline Hinnang Kaitsealadel [Complex Ecological Assessment of Water State in Protected Areas]*. Eesti TA Geoloogia Instituut, Tallinn, 45 pp. [in Estonian].
- Raukas, A. & Kink, H. 1993/94. *Veeseire kaitsealadel (1978–1992) [Water Monitoring in Protected Areas (1978–1992)]*. Nigula RLKA. Contract Work No. 7, Eesti TA Geoloogia Instituut, Tallinn, 48 pp. [in Estonian].
- Rydin, H. & Jeglum, J. 2006. (With contribution by Hooijer, A., Clarkson, B. R., Clarkson, B. D., Mauquoy, D. & Bennet, K. D). *The Biology of Peatlands*. Oxford University Press, 343 pp.
- Thompson, J. A., Bell, J. C. & Butler, C. A. 2001. Digital elevation model resolution: effects on terrain attribute calculation and quantitative soil-landscape modelling. *Geoderma*, **100**, 67–89.

LiDAR-andmetel põhinev Nigula soo topo-hüdroloogiline modelleerimine Edela-Eestis

Elve Lode ja Meelis Leivits

Veedirektiivist lähtuvalt on soomaastike valglatega seotud veeressursside kvaliteedi ja kvantiteedi andmestik oluline veemajanduskavade koostamisel. Vaatamata olemasolevatele pinnavee valglate jaotusmudelitele, on soode valglate piiritlemine siiani raskendatud nende suhteliselt tasandikulise, kuid samal ajal mikrovormiderikka mustriisuse tõttu.

Käesoleva töö raames LiDAR-andmestiku baasil loodud kõrgusmodelite (DEM-ide) topo-hüdroloogiline analüüs on esimene selline rakendus soolale. Erinevate algoritmidega (st TIN-, IDW-, MIN-, MAX-) genereeritud DEM-ide reljeefianalüüsist lähtuvalt sobivad soopinna üldiste/keskmiste topograafiliste parameetrite arvutamiseks kõik erineva piksli suurustega (st 1, 2, 5 ja 10 m) genereeritud DEM-id. Erineva piksli suurusega TIN-DEM-idest genereeritud Kaldvarjutuse (*HillShade*) kihtide võrdlemine viitas saadud kihtide piksli skaala tundlikkusele, millest tulenevalt on Nigula soo maastikulise tasandi topo-hüdroloogilise modelleerimise tarbeks enam sobivad DEM-id piksli suurusega 5 ja 10 m ning mikrovormide ja ökotoobi tasandi tarbeks suure tõenäosusega DEM-id piksli suurusega 1 ning 2 m. *Eukleidese kauguse* analüüs näitas vähimaid erinevusi TIN- ja IDW-DEM-ide baasil saadud soopinna topograafilistes tulemustes; EMP-DEM-iga aga rohkem sarnaseid keskmisi maastikulise tasandi tulemusi andis MIN-DEM-i reljeefianalüüs. MAX- ja MIN-DEM-ide lahutustehtest genereeritud kihil on selgelt eristatav soola kraavivõrgustik ning soola taimkatte vertikaalse skaala erinevate tasandite katvuse muster.

Modelleeritud soovalgate jaotuse ja koguste tulemused soo pinnal olid kasutatud piksli suuruse ning Piksli täitmise (*Pour point filling*) protseduuri tundlikud. Erinevate modelleerimissisendite puhul saadud soovalgate jaotusmustrite võrdlemisel prevaleeris Nigula soolal lõuna-edela väljavoolu orienteeritusega valglate grupp, pindalalise katvusega 58% soolast, millele järgnesid põhja-kirde, ida-kagu ja lääne orienteeritusega valglate grupid vastavate pindalaliste katvustega 23%, 11% ning 8% soolast. Kõige tihedama valglate jaotusmustriga oli järsema nõlvusega ja lääne orienteeritusega ning kõige hõredama mustriga tasased põhja-kirde orienteeritusega valglate grupp.